CHAPTER 3

BACKGROUND THEORY OF FRACTURE MECHANICS

3.1 Introduction

As pointed out in Sect. 1.2, understanding the mechanics and mechanisms of fracture in HAp, is critical to the prevention of catastrophic failure , and to the development of HAp implants with optimal strength properties. In this chapter, we will provide the theoretical background of fracture mechanics which will later be used in the fracture properties analysis of HAp.

Investigations on deformation and fracture properties of ceramics indicated that brittleness is an inherent property of ceramics. The stress necessary to cause such rupture varies from material to material according to the type of interatomic potential function. Fracture is envisaged as a simultaneous rupture of all bonds across the separation plane and thus the cohesive bond strength determines the intrinsic strength of ceramics. Practically, strength which is the critical tensile stress causing failure, are found to be at least two orders of magnitude less than the calculated intrinsic strength. Griffith was the first to recognize that flaws are responsible for the observed low strength. These flaws may be in the form of machining damage, grain boundary fissures, processing defects, (pores or inclusion), etc. Brittle fracture is usually triggered in ceramics by acting at the site of a flaw which intensifies the applied stress locally. Thus brittle fracture occures by a sequential bond rupture rather than the simultaneous separation.

Griffith's 1920 paper(3) which fundamentally rooted in the laws of classical mechanics and thermodynamics made two major contributions to the theory of strength of brittle ceramics: (i) brittle ceramics contain flaw which act as initiating centers for crack growth , (ii) the propagation of cracks proceeds in accordance with a balance between "riving" forces (associated with mechanical energy release) and " resisting " forces (associated with creation of crack surface area). The first of these, was to lead, ultimately, to a realization that material strength is governed by a wide range of intrinsic and extrinsic factors, embracing details of

microstructure (from the level of the cohesive bond to that of larger-scale features such as grains, inclusions and voids) and material history (mechanical,thermal and chemical). The second contribution, representing a statement of the first law of thermodynamics, was developed later by Irwin and others into a firmly-based analytic tool for evaluating the mechanics of crack propagation.

It should be reemphasized that strength is not a material constant. It is a measure of both intrinsic (material) and extrinsic (flaw) paramaters. The principal material parameter controlling strength properties of ceramics is the toughness, which is a measure of the resistance of material to flaw extension due to the many possible stresses imposed on the flaw. Fracture mechanics can be used to separate the material toughness from the flaw size distribution in the body. Because ceramics failure occurs from the most severe flaws in a wide distribution of flaws, this separation is important in understanding the fracture process. A ceramic component will fracture from the flaw where stresses acting at that location combine with the flaw severity to cause the flaw to grow. It is the presence of the flaw in the material which magnifies the applied stress to a value that causes the atomic bonds at the tip of the flaw to break.

3.2 Theoretical Framework of Fracture Mechanics

Modern-day theories of the strength of brittle materials stem from the Griffith energy balance description of fracture processes. Griffith regarded a cracked body as a thermodynamic system. The essential elements of his model are shown in Fig.3.1. A continuous, isotropic, homogeneous, linear elastic body containing an internal crack of length 2c is subjected to applied loading at its outer boundary. The total energy of the cracked body is made up of two components, the mechanical energy, U_M, and the surface work, U_S : $U = U_M + U_S$. The mechanical energy term, U_M, may in turn be broken down into two subcomponents, i.e. $U_M = -W_A + U_E$, where W_A is the work done by the applied loads in displacing the outer boundary and U_E is the stored elastic energy in the body. The surface energy term, U_S, is simply the
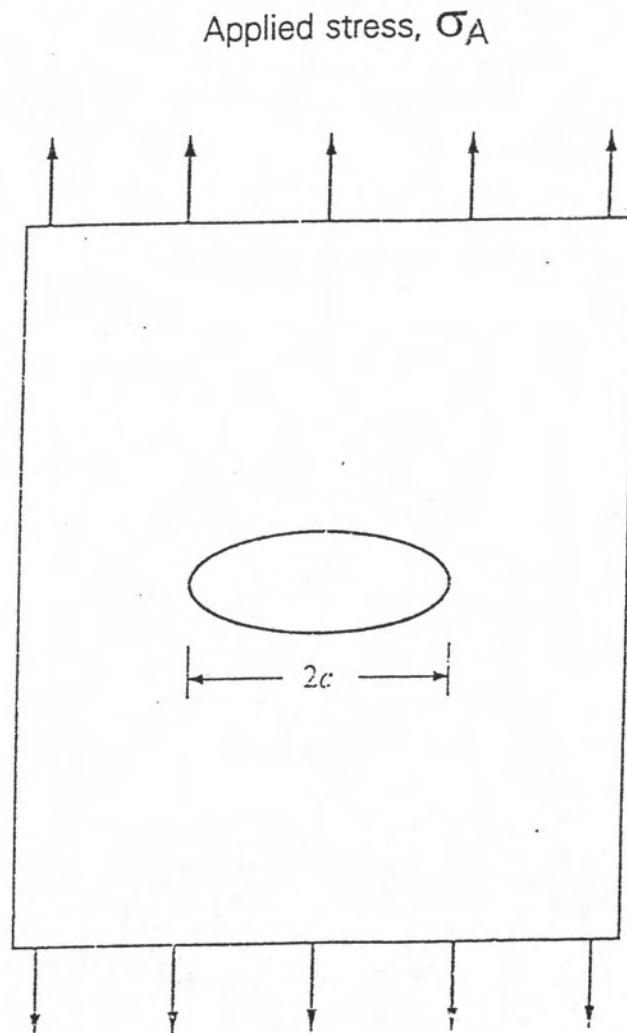
Applied stress, σ_A

Fig. 3.1 Schematic of plate containing crack of characteristic dimension 2c, subjected to uniform applied tension σ_A.

work to create the new crack faces. A state of equilibrium is reached when the energy has a stationary value with respect to any virtual change in crack area C, i.e.

$$dU/dC = dU_M/dC + dU_S/dC = 0 \qquad\qquad (3.1)$$

It is convenient to define the quantities

$$G = - dU_M/dC \qquad\qquad (3.2\ a)$$

and

$$-R = - dU_S/dC \qquad\qquad (3.2\ b)$$

so that Eq.(3.1) reduces to

$$G = G_c = R , \qquad\qquad (3.3)$$

where subscript c denotes the critical state in which the equilibrium crack is on the verge of extension : G is Irwin's mechanical energy release rate (25): it characterizes the forces that drive the crack. R characterizes the resistance forces associated with the surface formation processes. Of these two quantities, only R relates directly to intrinsic properties of the material.

Another fracture parameter, which is a convenient parameter for characterizing the crack driving force, is the stress intensity factor, K. This parameter takes us one step closer to the critical crack tip region. K is introduced into the fracture mechanics via an investigation of the manner in which an equilibrium crack modifies the stress field in an elastically - loaded solid (Fig. 3.2) :

$$\sigma_{ij} = K (\sigma_a, c) g_{ij}(\theta)/ (2\pi r)^{1/2} , \qquad\qquad (3.4)$$
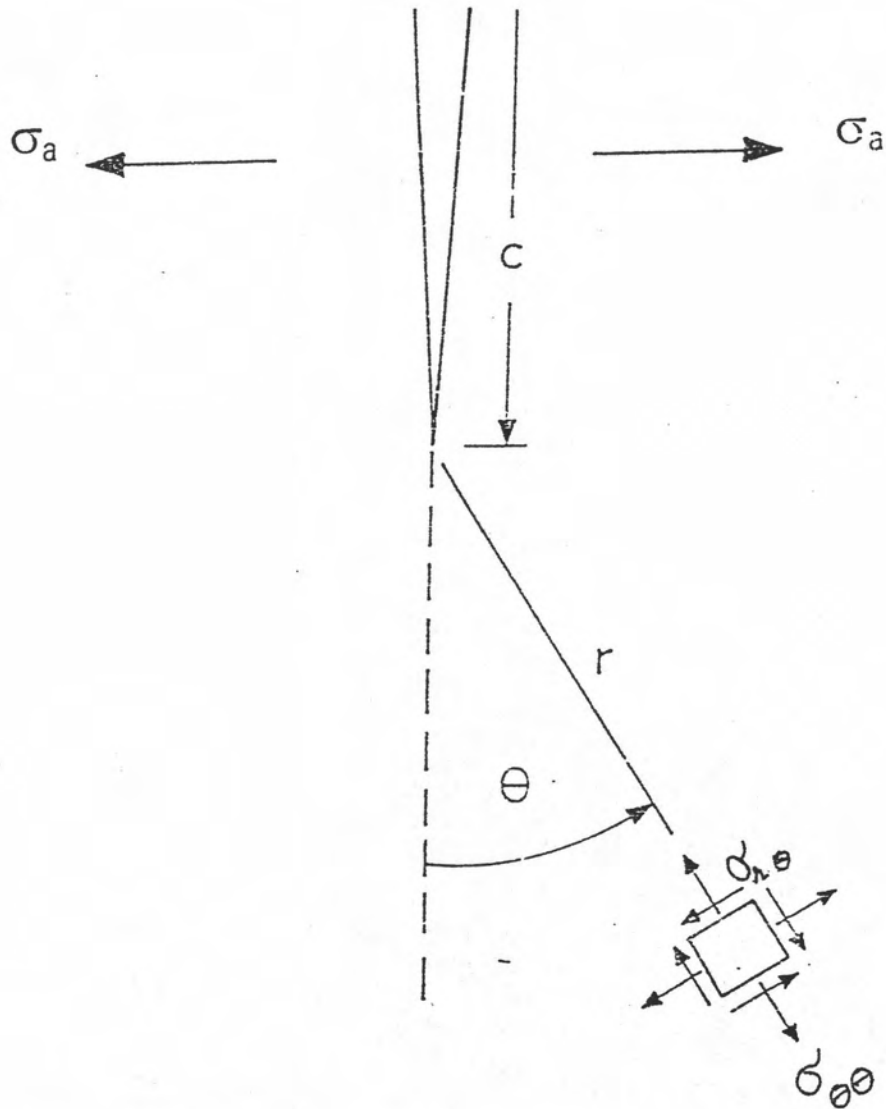
Fig. 3.2 crack-tip stress fields showing polar-coordinate components. σ_a and c spectively characterize the applied stress and scale of cracking.

where σ_a is an applied stress, c is a crack dimension, g_{ij} are angular functions, and r is the distance measured away from the crack tip into unbroken material. Thus K is defined as the slope of a plot of crack tip stress versus the distance from the crack tip r. (For a more detailed discussion see Lawn and Wilshaw (26) and Irwin and Paris (27)). K uniquely determines the intensity of the stress field about the crack tip and thus represents the crack driving force. K is an extremely powerful parameter in general fracture mechanics analysis. Relating as closely as it does to stress, it retains the major advantage of superposibility which is characteristic of linear properties. This additive property of K is of distinct advantage in determining the net mechanical force on the crack system.

The stress intensity factor can be demonstrated to bear a certain equivalence to the previously defined crack extension force, G. This is done by considering a virtual displacement of the crack tip; the mechanical energy release during such a displacement is then calculable in term of the stress components in Eq.(3.4) (26). For the opening mode fracture in which ceramics tend to fracture almost exclusively under this mode, the operation gives[*]

$$ G = K^2 / E $$

(3.5)

To analyse the crack response of a given crack loading system, one begins with the computation of the driving force on the crack system, either G or K . After the parameter G or K is established in terms of an applied stress σ_a and crack length c , we must then ask whether its value at a given load and crack length is sufficient to drive the crack, i.e. we need a fracture criterion. The Griffith energy balance concept, as having been expressed where E is the stiffness constant. mathematically in Eq. (3.3), tells us when a crack is on the verge of extension under essentially equilibrium condition : $G = G_c = R$. Such condition are usually

---

[*]This result is for plane stress conditions. For plane strain , E in

Eq.(3.5) must be replaced by $E/(1-\nu^2)$, where ν is Poisson's ratio.

realised in vacuum or in chemically inert environments or at low temperatures . For ideally brittle solids , $U_S = 2\gamma C$, where γ is the fracture surface energy and C the crack area, therefore

$$R = 2\gamma \qquad\qquad (3.6)$$

In accordance with Eq.(3.5), the equilibrium crack extension criterion may equally will be expressed in terms of a stress intensity factor as

$$K = K_c = T \qquad\qquad (3.7)$$

where T is interpreted as a material toughness parameter.
and

$$T = (2RE)^{1/2} \qquad\qquad (3.8)$$

It is well known from studies on more traditonal materials (metals and polymers) that the work required to create new crack area can exceed the reversible surface energy γ, sometimes by several orders of Eqs. (3.6) and (3.7) may be preserved by replacing γ with an effective fracture surface energy Γ, where it is now understood that the nowth is irreversible. For ceramics at room temperature the lack of intrinsic ductility severely limits he magnitude of the dissipative effect; the approximate range of relative energy terms is $1 < \Gamma/\gamma < 10$. There nevertheless exists some scope, within this range of values, forsignificant achievements in the design of relatively tough ceramic materials by control of fabrications variables, especily in relation to the microstructure which we aim to examine its effect on HAp in this work.

It is important to note that the equilibrium crack law embodied in Eqs.(3.6) and (3.7) relates to crack extension, but makes no statement as to whether this extension is unstable or stable (28). For the idealised crack configuration originally considered by Griffith, that of an otherwise stress-free crack in a homogeneous body loaded in uniform tension, the equilibrium

state is in fact unstable, so failure can be identified with the attainment of a critical G_c or K_c. However, there are many loading configuration in which the equilibrium crack states are stable, such that extension occurs only in response to a continual increase in the applied driving force. Hence, in general $G = G_c$ or $K = K_c$ constitutes a necessary but not sufficient condition for failure; an additional instability requrement must also be satified. It is possible , for instance, to concieve of loading configurations for which the equilibrium crack begins its extension in a stable mode and , after a significant increase in the applied load level,becomes unstable at a later stage of development (29).

To determine the nature of the equilibrium we have to consider the second derivative of energy, d^2U/dC^2. The system is unstable or stable depending on whether this second derivative is less than or greater than zero. In terms of Eq.(3.1) and (3.2) ,we obtain

$$dG/dC > dR/dC \quad \text{(unstable)} , \qquad\qquad (3.9\ a)$$

$$dG/dC < dR/dC \quad \text{(stable)} . \qquad\qquad (3.9\ b)$$

In the event of R independent of C the right side of Eq.(3.9) is zero; then (and only then) the stability is determined exclusively by whether G is an increasing or decreasing function of C. Likewise,the stability relations of Eq.(3.9) for such equilibrium states transform to

$$dK/dC > dT/dC \quad \text{(unstable)} , \qquad\qquad (3.10\ a)$$

$$dK/dC < dT/dC \quad \text{(stable)} . \qquad\qquad (3.10\ b)$$

Again, if T turns out to be independent of C the stability is determined exclusively by the functional dependence of $K(C)$. Thus, if there are internal contributions, K_i ,to the crack driving force, we may superpose these linearly onto the true applied loading contribution, K_a, to get Eq.(3.7)

$$K = K_a + \Sigma K_i \qquad . \qquad\qquad (3.11)$$

K is the effective driving force felt at crack tip. The K_i terms in Eq.(3.11) can be viewed as having a shielding or antishielding influence on the transmission of externally applied stresses to the crack tip, depending on whether the signs are negative or positive. It is generally possible to express the internal terms as an integral over traction $\sigma_i(X)$ at the crack interface,

$$K_i = \int_0^C g(C,X) \, \sigma_i(X) \, dX \quad , \qquad\qquad (3.12)$$

where X is an area coordinate measured from the origin in the crack plane and $g(C,X)$ is an appropriate Green's function. The conditions for instability or stability in Eq.(3.10) translate to

$$dK/dC = dK_a/dC + d(\Sigma K_i)/dC \gtrless 0 \qquad\qquad (3.13)$$

Inserting Eq.(3.11) in Eq.(3.7) gives the modified equilibrium relation

$$K = K_a + \Sigma K_i = T_o \qquad , \qquad\qquad (3.14)$$

where the subscript zero on the T term denotes a material-invariant toughness, i.e. the toughness if the K_i terms were entirely absent. Of the individual K terms in Eq.(3.14), it is only K_a which is monitored directly, via the external loading system in a fracture test. Consequently, it has become commom practice to regard the K_i terms implicitly as part of the toughness characteristic. This pliilosophy is formalized by rewriting Eq.(3.14) in the form (28)

$$K_a(C) = T(C) = T_o - \Sigma K_i \qquad . \qquad\qquad (3.15)$$

The modified equilibrium relation (Eq.(3.15)) retains the same simple form as Eq.(3.14), except that now T cannot be regarded as a material invarient. The instability/stability condition of Eq.(3.10) now become

$$dK_a/dC \geq dT/dC \qquad (3.16)$$

For the special case of a straight crack, where length c is sufficient to define the crack area (C).

In many ceamics cracks can extend at subcritical stress levels, especially in the presence of reactive chemical environments, e.g. water. Chemical processes activate bond rupture at the crack tip and the crack can therefore extend slowly in response to the environment and applied stress at subcritical leveis, i.e. at $K < K_c$. A major feature of this type of fracture is its time dependence. Extension occurs at a rate which depends sensitively on the magnitude of the applied stress. Other variables are the concentration of chemically active species, crack length, c , and temperature , T . The crack extension condition is according expressible in terms of a crack velocity function

$$v = dc/dt = v(G \text{ or } K, c, T), \qquad (3.17)$$

in the region G or $K < G_c$ or K_c

3.3 Crack Systems Produced by Sharp Indenters

Having provided a background of fracture mechanics framework, we shall now focus our attention to fracture behaviours produced by sharp indenters. Sharp indenters like the Vickers* or Knoop** indenter used in hardness testing produce two basics types of crack pattern : radial-median and lateral (26). Figs. 3.3 a and 3.3 b show the cross-sectional together

----

* A Vickers indenter is a squared-base diamond pyramid with an angle of 130° between opposite faces of the pyramid and 148° between the pyramid edges.

** A Knoop indenter is a rhombic-based diamond pyramid with a ratio between long and short diagonals of about 7 to 1. The pyramid shape used has an included longitudinal angle of 172°30' and an included transverse angle of 130°0'.
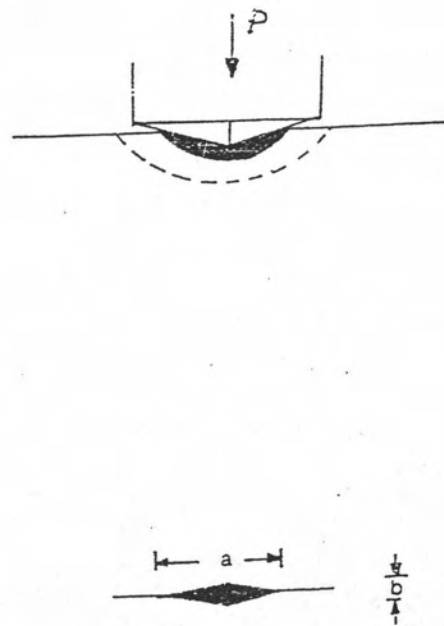
(A)
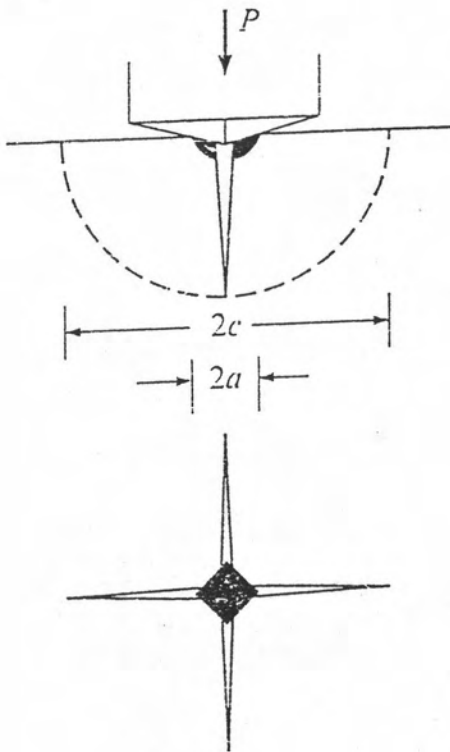
(B)

Fig. 3.3 Show cross-sectional together with top schematic of

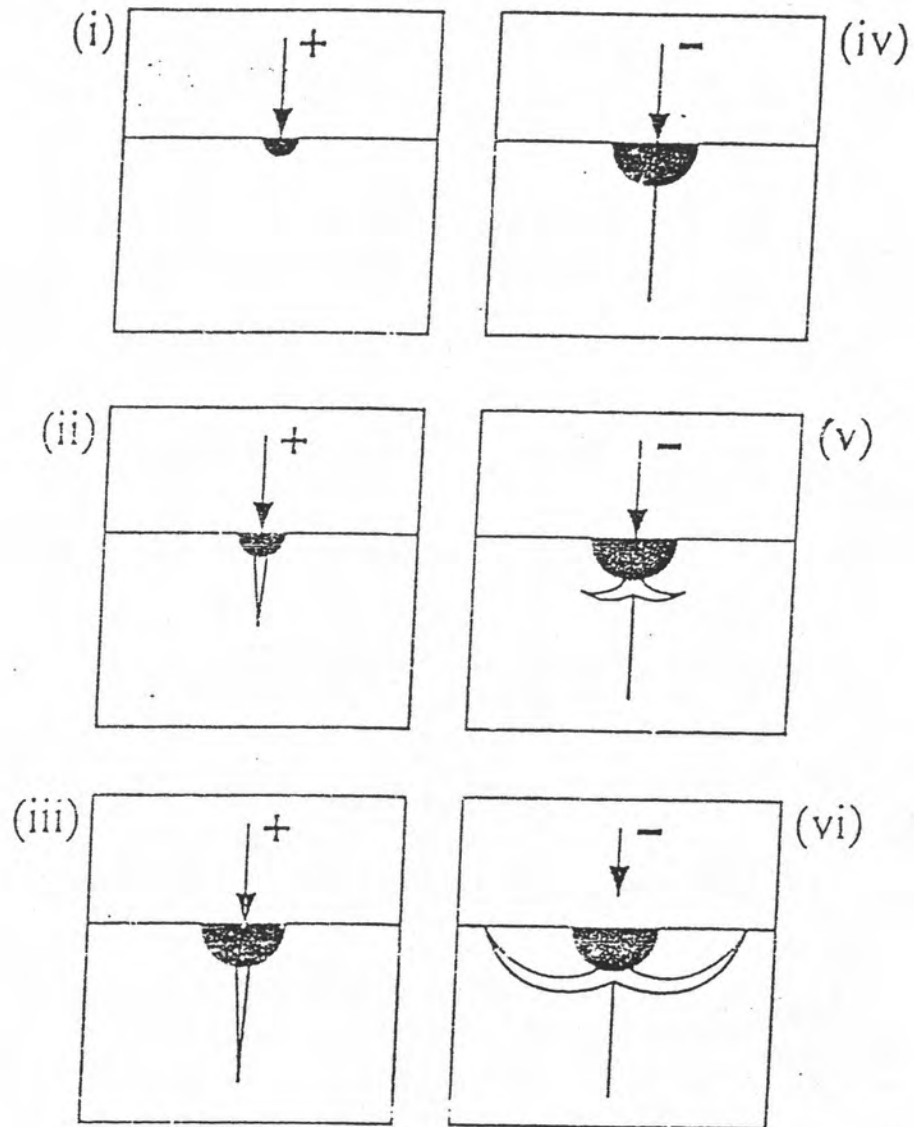(A) Vickers damage   (B) Kncop damage.

Fig. 3.4 Evolution of radial- median and lateral crack systems during complete loading (+) and unloading (-) cycle. Dark region denotes irreversible deformation zone.

with the top schematic of the Vickers and Knoop damages typically observed in ceramics respectively. Fig.3.4 depicts the evolution of these crack systems: (i) the sharp point induces inelastics, irreversible deformation;(ii) at a critical load one or more nascent flaws within the deformation zone become unstable, and pop-in to form subsurface radial cracks on tensile median planes, i.e. planes containning the load axis (and,usually,some line of stress concentration, e.g. impression diagonal or cleavage-plane trace in the specimen surface); (iii) on increased loading, the crack propagates incrementally downward; (iv) on unloading, the median cracks close up below the surface but simultaneously open up in the residual tensile field at the surface as the contact recovers its elastic component; (v) just prior to removal of indenter the residual field becomes dominant, further expanding the surface radials and initiating a second system of sideways spreading, saucer-like lateral cracks near the base of the deformation zone; (vi) the expansion continues until indenter removal is complete, both crack systems ultimately tending to half-pennies centred about the load point. The lateral crack system forming in a saucer-like fracture approximately parallel to the surface can cause

The damage pattern produced by the sharp indenter has now been well accepted as a powerful tool for determining the fracture properties of ceramics. It serves a simple microprobe for determining material hardness, stiffness, toughness, crack-velocity exponent, etc. More importantly, it is used as a means of providing insight into the fundamental mechanics of failure. The sharp indenter provides a small precrack from which the specimen fails. This indentation precrack can be accurately positioned on any prospective test surface and its scale is readily controlled to a high degree of reproducibility via the indentation load. By adjusting the indentation load, the size of tne precrack can be controlled with great accuracy. From a series of tests over a wide range of indentation loads, one can measure the strength systematically as a function of starting crack size. Although the indentation cracks are artificially introduced entities, there is a considerable evidence that they do indeed simulate the essential qualities of naturally occurring surface flaws in ceramics components (30): cracks introduced by scratching, surface finishing process , and spurious articlecontact are just a few pertinent examples . The hipping, and is therefore particularly pertinent to the problem of surface wear and erosion; the median-radial crack system is more likely source of component failure.

great appeal of the indentation methodlogy is its versatility, control, and simplicity, requiring only access to routine hardness testing apparatus.

Now we examine the mechanics of contact. For rigid, fixed profile pyramid (Vicker or Knoop) indenters where geometrical similarity prevails, we have an elastic-plastic of contact pressure

$$p_o = P/\alpha_0 a^2 = H \qquad (3.18)$$

where H defines the indentation hardness, P the contact load, a a characteristic dimension of the impression , and α_o an indenter constant.

3.4 Residual Contact Stress

We will now consider the role of residual contact stress, due to the mismatch between central deformation zone and surrounding elastic matrix, play in the fracture evolution. In this section, we will concentrate only in the case of fracture evolution in a material of constant toughness. By virtue of the plastic contact process, the field which drives the indentation cracks contains both an elastic (reversible) and a residual (irreversible) component. The elastic component can be represented by a" Boussinesq " point-load elasticity solution, shown in Fig 3.5 b by means of stress contours in the median lane. Therefore during the loading half-cycle the tensile component of the elastic field enhances downwards crack extension but is constrained somewhat at the surface by the compressive component of the elastic field, thus cracks formed during the loading half-cycle is of the elastic component that can be written as $K_e = X_e(\phi) P / c^{3/2}$ where $X_e(\phi)$ is an angular function , changing from positive (tensile) at $\phi = 0$ to negative (compressive) at $\phi = +90^o$, and its magnetude depends cn the ratio of crack size to plastic zone size, c/b. The residual component aries from mismatch stress associated with stress/strain incompatibility between central deformation zone and surrounding elastic matrix and is characterized by a residual centre-opening force in Fig. 3.5 c . Thus this residual field is superimposed on the tensile component of elastic field in driving downwards
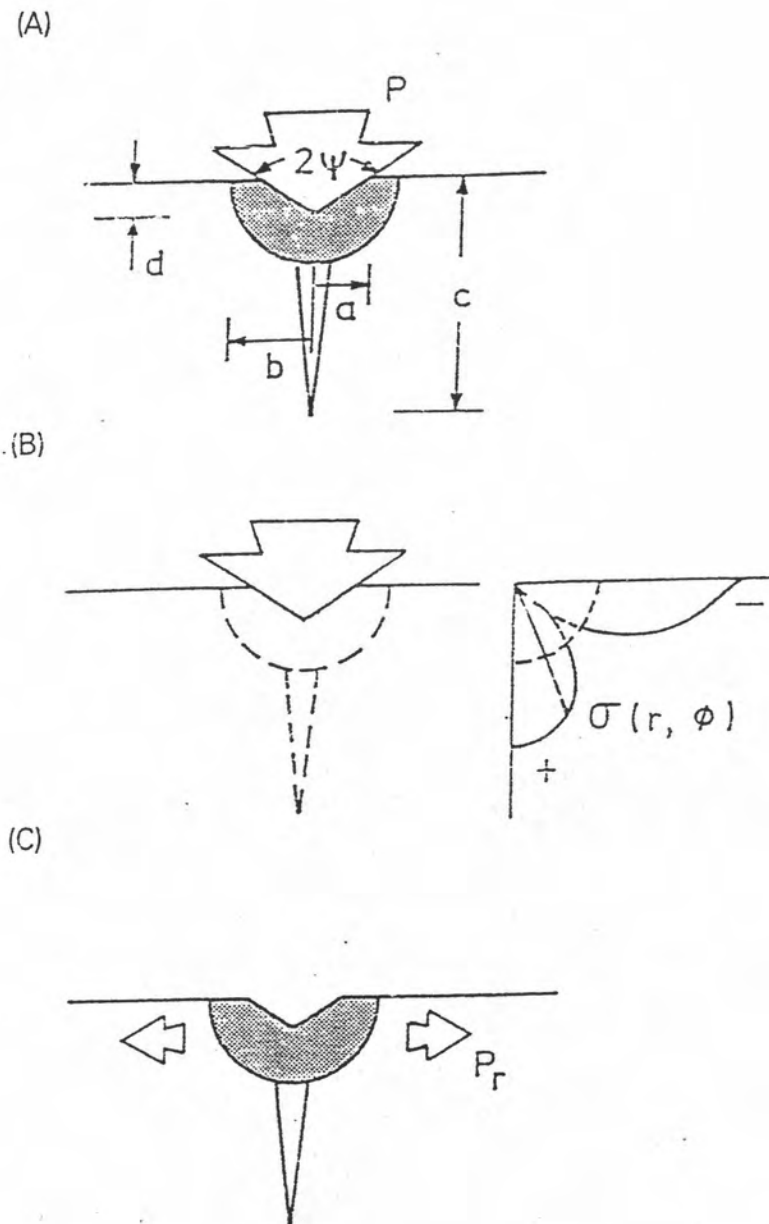
(A)

(B)

(C)

Fig. 3.5 Median/radial crack system, showing (A) elastic/plastic configuration at full load subdivided into (B) elastic component at full load plus (C) residual compmnent at complete unload.

crack extension during the loading half cycle. The stress intensity factor of the residual component can be written as (31) $K_r = \chi_r P/c^{3/2}$, where χ_r is the irreversibility of residual term for the radial component and its magnitude depends on ratio of Young's modulus to hardness, E/H ,

$$\chi_r = \xi(E/H)^{1/2} \quad , \tag{3.19}$$

where ξ is a material-independent constant for Vickers-produced radial / median cracks. Accordingly, the stress intensity factor equation for the median crack which fully forms during the loading half-cycle can be written as

$$K = (\chi_e + \chi_r) P/c^{3/2} \quad . \tag{3.20}$$

During the unloading half-cycle, the mponent of elastic field is released, the residual component accordingly provides the primary driving force and the crack is thus driven radially outwards. Thus the stress intensity factor can be written as

$$K_r = \chi_r P/c^{3/2} = \xi (E/H)^{1/2} P/c^{3/2} \quad . \tag{3.21}$$

The condition for equilibrium growth of the cracks after completion of contact cycle is obtained by equating the net stress intensity factor, K , to the intrinsic material toughness T_0. Then the toughness parameter T_0 of the material can be evaluated from the direct measurement of sizes of the equilibrium radial cracks, c_0 , using the relation

$$T_0 = \xi (E/H)^{1/2}(P/c^{3/2}) \quad . \tag{3.22}$$

The residual contact stress is felt not only in the development of the median-radial cracks, but also persist through subsequent strength testing in a way that stabilized the crack. Fig. 3.6 is a schematic diagram showing a two-step procedure in which the indentation crack is
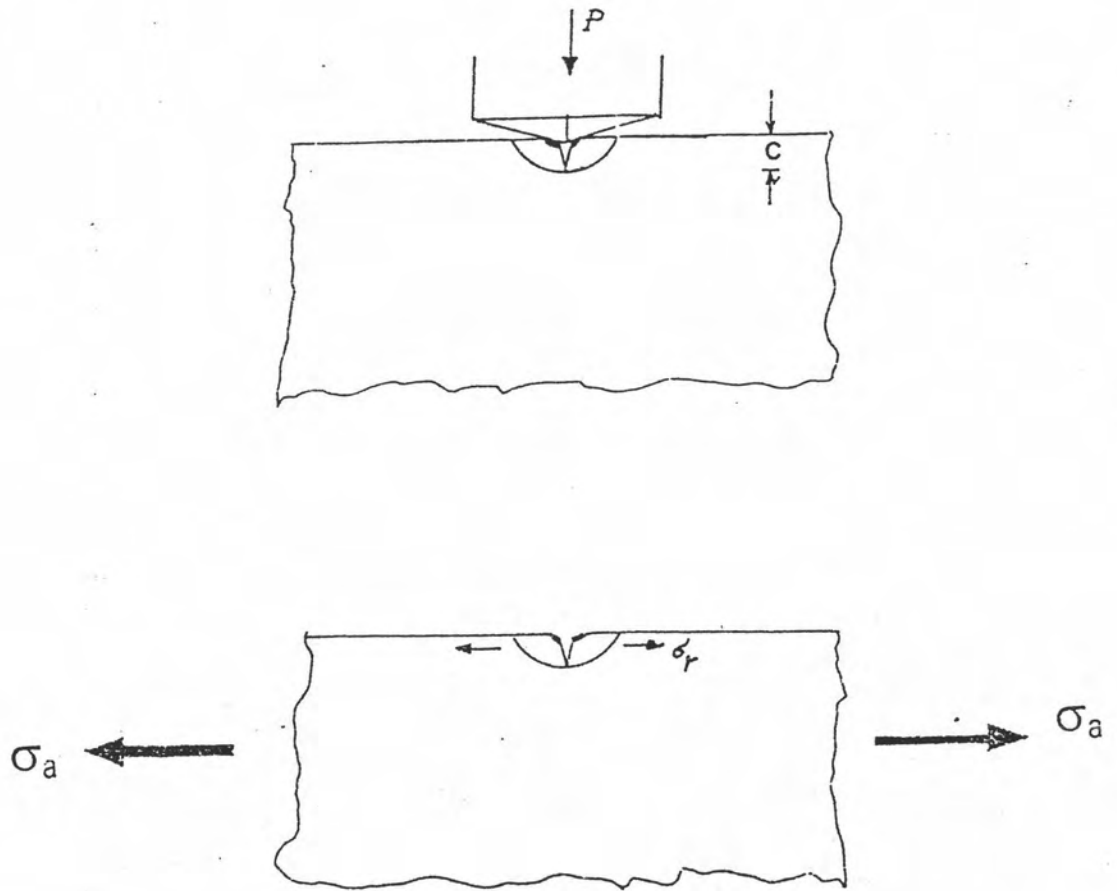
Fig. 3.6 Schematic of indentation / strength sequence. (A) Vickers indenter, peak load P, generates radial-median crack of characteristic dimension c. (B) Tensile stress σ_a combines with residual contact stress σ_r to drive crack to failure configuration

placed in the test surface as a strength-controlled crack : the specimen is first loaded with a sharp indenter to introduce a well-defined crack system into the surface, and is subsequently loaded to failure by an applied tensile stress σ_a . As pointed cut above, the radial crack experiences, a substantial residual opening force which is quantified by a stress intensity factor of the form given in Eq.(3.21),

$$K_r = \chi_r P/c^{3/2} \quad . \tag{3.23}$$

In the tensile loading stage, Fig 3.6 b , an applied stress σ_a augments the residual driving force. The appropriate stress intensity factor for this second force is of the form

$$K_a = \sigma_a (\pi \Omega c)^{1/2} \quad , \tag{3.24}$$

where Ω is a crack-geometry parameter. Thus the radial crack in a material of constant toughness is subjected to a net stress intensity factor

$$K = \chi_r P/c^{3/2} + \sigma_a (\pi \Omega c)^{1/2} . \tag{3.25}$$

For equilibrium growth, $K = T_o$ (Sect.3.2),Eq.(3.14) may be solved explicity for the functional dependence of applied stress on the crack size,

$$\sigma_a = [K_c/(\pi \Omega c)^{1/2}][1 - \chi_r P/(K_c c^{3/2})] \quad . \tag{3.26}$$

This function is plotted in Fig. 3.7 for nonzero and zero χ_r.

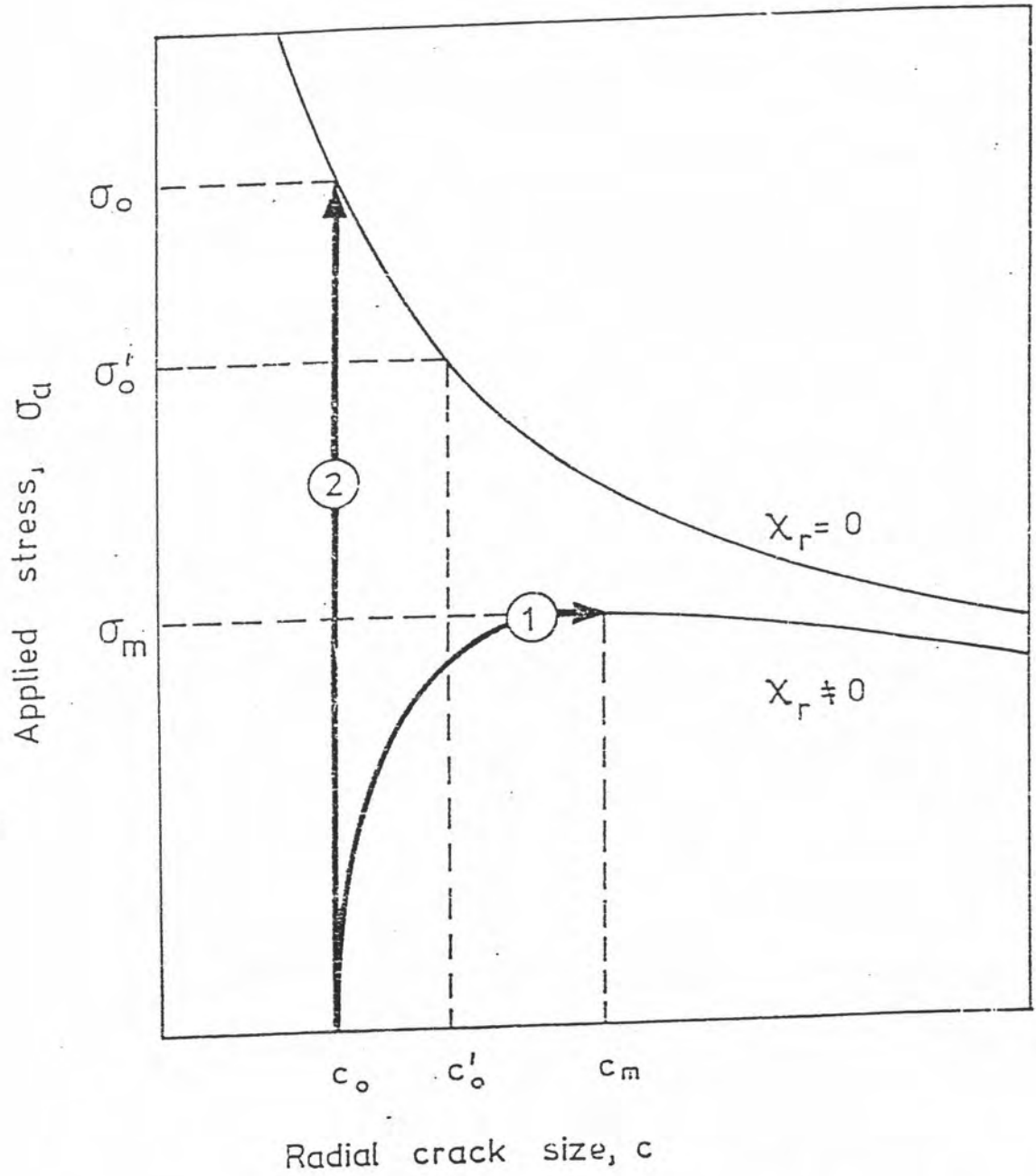For $\chi_r > 0$, the $\sigma_a(c)$ curve (Fig. 3.7) has a maximum $(d\sigma_a/dc = 0)$ at

Fig. 3.7 Plot of function $\sigma_a(c)$ in Eq. (3.26) for radial cracks with and without residual contact stresses. Curve 1 and 2 indicate respective paths to failure under equilibrium fracture conditions.

$$\sigma_m = 3K_c/4(\pi\Omega c_m)^{1/2} , \qquad\qquad (3.27\ a)$$

$$c_m = (4\chi_r P/K_c)^{2/3} . \qquad\qquad (3.27\ b)$$

For $c < c_m$ the crack is stable ($d\sigma_a/dc > 0$), for $c > c_m$ it is unstable ($d\sigma_a/dc < 0$). The condition for failure is that the system attains a configuration on the unstable branch of the $\sigma_a(c)$ curve. The equilibrium strength relation for any given indentation situation will then depend on the size of the initial crack relative to the value c_m. Comparing the maximum crack size, $c = c_m$ (Eq. 2.27 b), with the initial crack size $c = c_o$ (Eq. 3.21), it follows that

$$c_m/c_o = 4^{2/3} = 2.52 . \qquad\qquad (3.28)$$

This indicates that, under equilibrium conditions, the initial crack undergoes substantial precursor stable growth, from c_o to c_m, in achieving an instability configuration at $\sigma_a = \sigma_m = \sigma^r_i$. The existence of this " energy barrier " to failure has been confirmed by direct observation of radial crack growth under inert conditions (vacuum or dry N_2 environment) in glass[32], silicon[33], and in several ceramics[34]. Eq.(3.27) thereby gives the inert, residual-stress-sensitive strength

$$\sigma^r_i = 3K_c/4(\pi\Omega c_m)^{1/2} = [27K_c/256\chi_r(\pi\Omega)^{3/2}P]^{1/3} . \quad (\chi_r > 0) \quad (3.29)$$

Substituting Eq.(3.19) into Eq.(3.29) gives

$$\sigma^r_i = [27K_c(H/E)^{1/2}/256\xi(\pi\Omega)^{3/2}P]^{1/3} . \quad (\chi_r > 0) \qquad (3.30)$$

For $\chi_r = 0$, i.e. in the limit of zero residual stress, Eq.(3.26) reduces to the conventional strength equation. The function $\sigma_a(c)$ has only an unstable branch (Fig. 3.7). Failure thus

occurs spontaneously at $\sigma_a = \sigma^0_i$, $c = c_o$, and Eq.(3.26) gives the appropriate inert,residual-stress-free streng

$$\sigma_i = K_c / (\pi \Omega c_o)^{1/2}. \qquad (\chi_r = 0) \qquad\qquad (3.31)$$

From the above formulation, it can be seen that the residual stresses accompanying radial cracks have important implications concerning the stability of the crack under tensile loadings, with consequent effects in the failure criteria. Because of the predicted existence of an energy barrier to failure, the initial crack size no longer plays a direct part in the strength determination: the strength is independent of whether the initial crack size corresponds to the true equilibrium value c_o or to a larger value c_o due to chemical enhancement prior to tensile loading, provided that $c_o < c_m$ (Fig. 3.7). This conclusion runs counter to the conventional strenght theory based on "ideal" Griffith flaws (i.e. no residual stress),in which flaw history can be a controlling factor (c.f. Eq.(3.31) and the constuction in Fig. 3.7 for zero χ_r). Besides this, it results in the reduction of the equilibrium failure stress. Eqs.(3 29) and (3.30) may be combined with Eq.(3.28) to obtain the strength ratio of indentation flaws with and without residual stresses:

$$\sigma^r_i/\sigma^0_i = (3/4)(c_o/c_m)^{1/2} = 0.47 \quad . \qquad\qquad (3.32)$$

Thus the presence of the residual field may reduce the equilibrium strength by more than a factor of two.

Generally, it is most convenient to plot indentation-strength data in the functional form $\sigma(P)$, in accordance with Eq.(3.19), using the independent variable P to characterize the flaw severity. Fig. 3.8 shows such a plot for three relatively homogeneous brittle solids. The data cut off abruptly at low load, where failure occurs from natural rather than indentation flaws. Apparent satisfaction of the $P^{-1/3}$ dependence in Eq.(3.19) for the data sets may be taken as validating the assumption of constant toughness T_o.
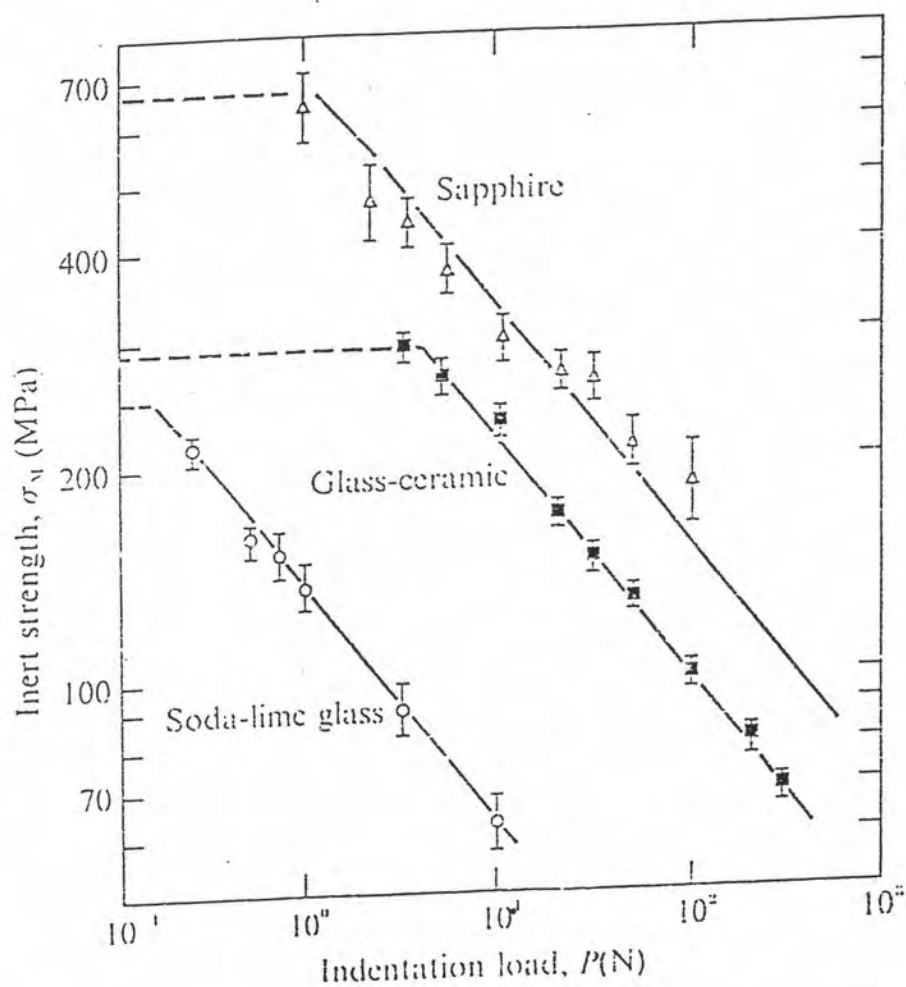
Fig. 3.8 Inert strength as function of Vickers indentation load for soda-lime glass, fine-grained cordierite glass-ceramic and monocrystal sapphire specimens with polished surfaces. All data points are failures from indentation sites. Error bars are standard deviation limits. Solid lines are fits with slope -1/3 in logarithmic coordinates. Dashed lines are natural flaw cut offs. (After R.F. Cook and D.B. Marshall (38))

3.5 Microstructure - Associated Stress

In the previous section, we have described fracture evolution in materials with constant toughness T_0. Many ceramics show a significant toughness increase with continued crack extension, the so called R-curve or T-curve behaviour, rather than a single-valued quantity. In this section, we will extend the analysis to such materials by incorporating the microstructural stress intensity factor, K_μ into the fracture mechanics analysis.

3.5.1 Crack Interface Bridging Stress

A substantial body of evidence now exists to demonstate that grain-localized bridging at the crack interface behind the advancing tip (35-47) is the principal mechanism of T-curve behaviour in the monophase , e.g. alumina , glassceramics, etc. The most definitive identification of the underlying mechanism responsible for the T-curve behaviour of monophase, nontransformable ceramics is the in-situ observations of crack evolution in a coarsed-grain alumina by Swanson et al (40). They used the tapered-cantilever beam specimens and the indented specimens and focused a microscope onto the controlled-crack site during stressing the specimen to failure. Such strength-controlled cracks were found to extend several times their original dimensions prior to failure. A high density of active regions where grains remained attached to both walls of the newly formed crack interface was found to leave behind the advancing crack front over many millimeters (Figs. 3.9 and 3.10), corresponding to the similar scale of its observed T-curve. Their studies demonstrated clearly that the partially attached grains exerted significant tractions on the crack wall behind the crack tip by a frictional pullout mechanism. Thus the enchanced stable crack growth prior to tradition strength theory based on the presumption of a single-valued toughness, was attributed to increasing interfacial restraints as more and more crack-interface grain-bridging sites were activated by the expanding crack. The crack-interface grain bridging sites behind the crack tip provided closure forces to the crack surfaces which shielded the crack tip from the applied stress. Subsequent extension to other ceramics confirmed the generality of the phenomenon(46).

Fig. 3.9 Refected light micrograph of mosaic of evolution in tapered-cantilever beam specimen of alumina. shown at six stages of loading. (After Swanson et al.(40)).
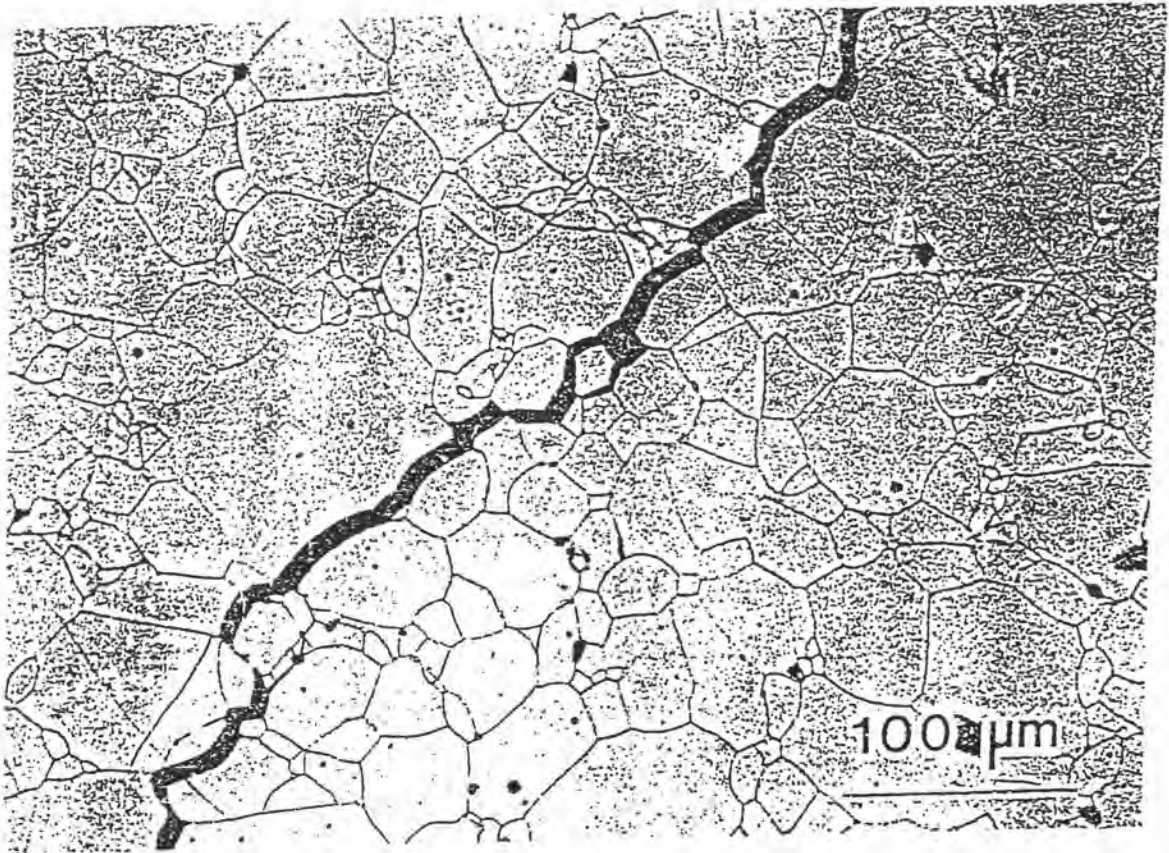
Fig. 3.10 Reflected light micrograph of an indentation crack in a fractured alumina disc.

(After Swan et al.(40))

We will now determine the micromechanics of grain interlocking and subsequent pullout (46) by considering a half-penny crack (radial c) evolve in a rectangular microstructure. The crack is assumed to begin its life as a flaw in a region of most favorable internal tension, + σ_R, (Fig.3.11a). Thereafter it is assummed to intersect bridging grains as it expands radially outward (Fig.3.11b,c). The grains which act as bridges are asumed to be those with compressive components of the residual stress field -σ_R, at transverse facets (Fig.3.11d). The problem is then to determine the closure stresses , p , exerted by the bridges in terms of crack-wall separation.

These stresses are governed by Coulombic friction that restricts the separation of bridging grain facets. At initial separation the bridging grains debond along the constrained facets and then pullout until final rupture at some ritical rupture strain. The constitutive relation between closure stress and (half-) crack-opening displacement, u , for a dominated pullout relation (41,46) can be written as

$$p(u) = p_m(1-u/u_l) \qquad\qquad (3.33)$$

where p_m is the maximum resistance stress (at u= 0) and u_l is the wall-wall half-displacement at bridge-matrix disengagement (at p=0). The essential material quantities in Eq. (3.33) are contained in the parameters (46) :

$$u_l = \in_l l/2 \qquad\qquad (3.34a)$$

$$p_m = (\alpha_\lambda \alpha_L \in_l \mu \sigma_R)(1-1/2\alpha_d^2) \qquad\qquad (3.34b)$$

with l grain size, μ friction coefficient, σ_R internal residual stress. The α and $\in$ terms are dimensionless constants for geometrically similar microstructures:
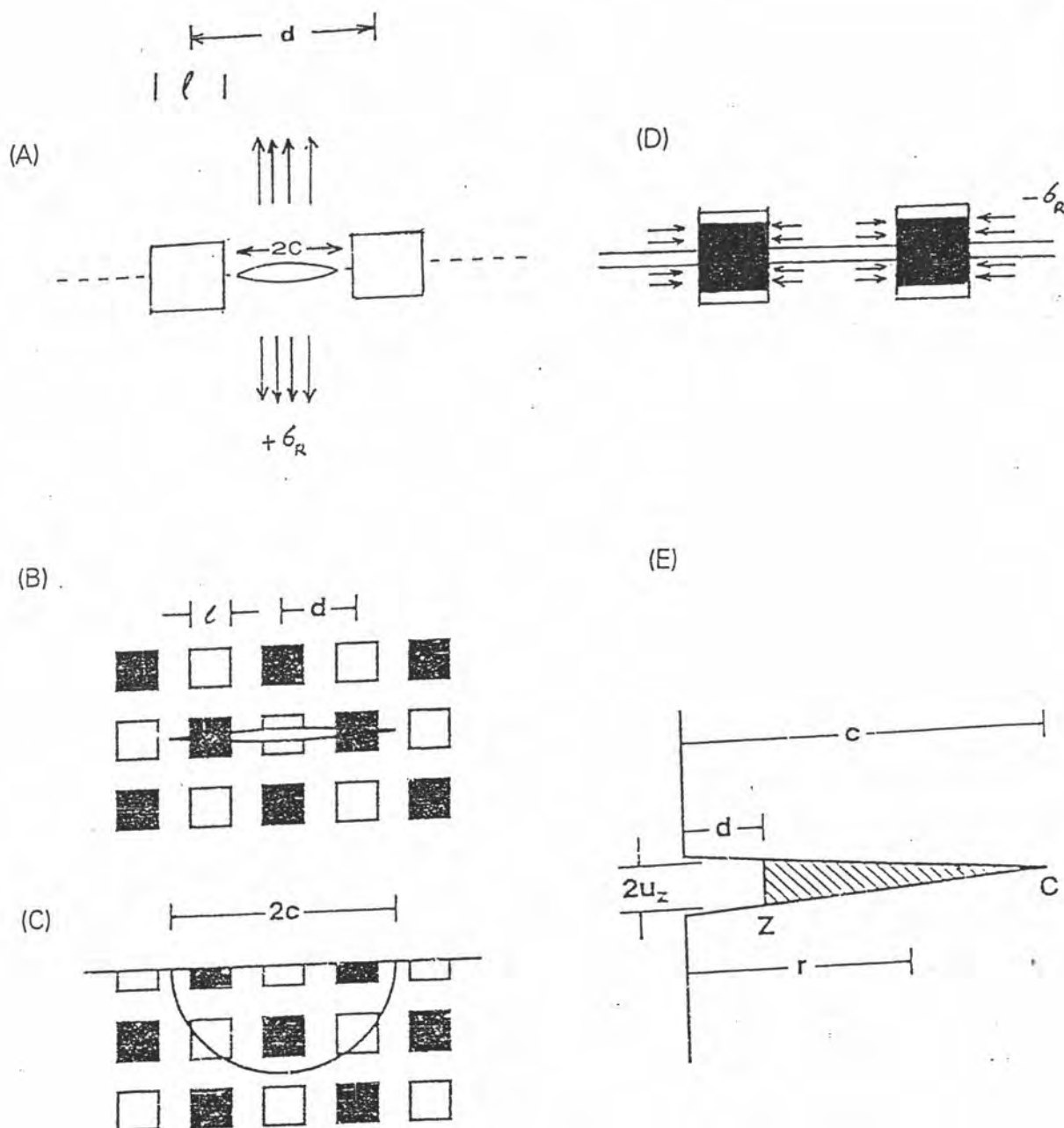
$$\alpha_\lambda = \lambda/l \qquad\qquad (3.35a)$$

Fig. 3.11 Microstructural model of grain briding for half-penny crack or characteristic dimension c in microstructure with bridging grain. Squares represents bridging grains(grain size l and bridging spacing d).(A) crack initiates in residual tensile field $+\sigma_R$ associated with thermal expansion mismatch (c<d), (B) in-plane view of crack extension into bridging field (c>d),(C) out-of-plane view of crack extension into bridging field (c>d)(D) grain pullout, (E) coordinate system for bridging zone.

$$\alpha_L = L/l \qquad\qquad (3.35b)$$

$$\alpha_d = d/l \qquad\qquad (3.35c)$$

$$\in_l = 2u_l/l \qquad\qquad (3.35d)$$

with λ the bridge cross-sectional perimeter, L the embedded grain length, d the bridge spacing. In Eq.(3.34) only the pullout distance u_l depends on the grain size ; the closure stress p_m is scale-invariant.The toughening associated with the bridging is calculated according to crack-size domain, as follows (41,42,46,48):

(i) Small cracks (c $\leq$ d) ; there is no bridge intersections. within this region the crack experiences only the matrix tensile stress, $+\sigma_R$. Assuming this field to be uniform, and using Eq. (3.4) we obtain

$$\bar{T}_\mu(c) = -K_\mu(c) = -\psi\sigma_R c^{1/2} \qquad\qquad (3.36)$$

where ψ is a geometry dependent coefficient. This T_μ term is not expected to be present in straight crack. where tensile and compressive facets average to zero stress along the crack front.

(ii) Intermediate cracks (c $\geq$ d, $0 \leq u \leq u_l$) : bridges intersected. There are two contributions to the toughness in this region, $T_\mu(c) = T_\mu'(c) + T_\mu''(c)$. The first is an opening post-intersection component from the persistent residual tensile stress field from (i) above,

$$T_\mu'(c) = -\psi\sigma_R c^{1/2} [1 - (1 - \alpha_d^2 l^2/c^2)^{1/2}]. \qquad\qquad (3.37)$$

The second is a countervailing closing component from the bridging traction, Eq. (3.33). This contribution is most readily evaluated as a J-integral in form of crack-resistance,

$$R_\mu^{''}(u) = 2\int_0^{u_z} p(u)du = 2p_m u_z(1-u_z/\in_l) \qquad (3.38)$$

The displacement $u_z = u_z(c)$ at the edge of the bridging zone (i.e. first bridge intersection at $c = d$, Fig. 3.11e) may be evaluated approximately from the Sneddon crack profile relation ("weak shielding" approximation)

$$u_z(c) = (\psi K_a/E')[(c^2-\alpha^2 d l^2; c]^{1/2} \qquad (3.39)$$

where $E' = E/(1-\nu^2)$.

The toughness $T_\mu^{''}(c)$ may be determined from the crack-resistance $R_\mu^{''}(c)$,

$$T_\mu^{''}(c) = E'^{1/2}\{ [R_\mu^{''}(c) + G_c]^{1/2} - (G_c)^{1/2} \}. \qquad (3.40)$$

This relation is implicit in $T_\mu^{''}$, so Eqs. (3.15),(3.38)-(3.40) must be solved simultaneously.

(iii)   Long cracks ($c >> d$, $u_z \geq u_l$) ; bridging zone is now of constant size and translating with the advancing crack. In this limit, $T_\mu' \to 0$ and the steady-state toughening increment is evaluated from Eq. (3.40) with $R_\mu^{''} = p_m \in_l/2$ from Eq.(3.38).

The inert strength of a ceramic material is determined by the condition for instability under essentially equilibrium condition: $dK_a/dc \geq dT/dc$ at $K_a(c) = T(c)$ (Eq.(3.16)). According to we can write the net stress intensity factor for controlled indentation radial cracks formed at contact load P and subsequently subjected to uniform tensile stress σ_a in form,

$$K(c) = K_a(c)+ K_r(c) = T(c) = T_0 + T_\mu(c) . \qquad (3.41)$$

Here $K_a(c) = \Omega\sigma_a c^{1/2}$ relates to the applied stress σ_a (Eq.(3.24)) (Ω a crack-geometry con.stant), $K_r(c) = \chi_r P/c^{3/2}$ to contact residual stress at indentation load P (Eq.(3.23)) (χ_r a contact constant). $K_a(c)$ and $K_r(c)$ are extrinsic driving forces on the crack system (positive). $T_\mu(c)$ is the contribution from internal grain-bridging restraints (Eq.(3.36),(3.37), (3.40)) which is an intrinsic resistive term (negative). T_0 is the intrinsic grain boundary toughness and is strictly independent of crack length and is strictly independent of crack length (9) so that $K(c)$ is an effective applied K-field. Failure at $c = c_m$, $\sigma_a = \sigma_m$ is then determined from the instability requirement $dK_a dc = dT/dc$ in Eq.(3.16), with proper allowance for pseudo failure states (see below). Generally, except for the simplest $T_\mu(c)$ functions, solving for $\sigma_m(p)$ in analogy to Eq.(3.27) requires numerical analysis.

Indentation-strength results for a coarse-grained alumina(single phase and equiaxed microstructure with grain size $I = 35$ μm.) with shielding by crack-interface bridging are plotted in Fig, 3.12. Data points represent confirmed failures from indentation flaws, the shaded band at left failures from natural flaws. The solid curve is a fit obtained by adjusting microstructural parameter μ, σ_R, $\in_I$ and α terms in Eq. (3.34), using numerical algorithm (49). The dashed σ_m $\propto$ $p^{-1/3}$ line from a fit of Eq.(3.30) to data for monocrystalline alumina (sapphire) establishes a comparative baseline. At decreasing P the data tend strongly to a plateau, asymptotic to the strength for failures from natural flaws. Fig. 3.13 shows T-curve which was deconvoluted from above fit in Fig. 3.12 by using Eq. (3.36)-(3.40).Note that the intrinsic material toughness initially diminished from $T = T_0$ with crack size, due to the action of the residual tensile field at $c \leq d$ (Fig. 3.13). After the first bridge intersection the toughness rises sharplyas a result of dominant frictional restraining stresses from the grain pullout. This rise continues as the bridging zone expands with crack extention,until the first bridge ultimately ruptures. At this point the bridging zone translates with the crack, and a steady state obtains at $T = T_\infty$. Fig 3.14 shows applied stress vs crack size for Vicker indentation in alumina, using parametric evaluations from Fig.(3.12) at a load well within the plateau region, $P = 2$ N. Two stabilising branches are now apparent (c.f. Fig. 3.7), one on either side of the first bridge activation at $c = d$: that at $c < d$ relates to a dominant $K_r(c)$ function (small-crack,positive
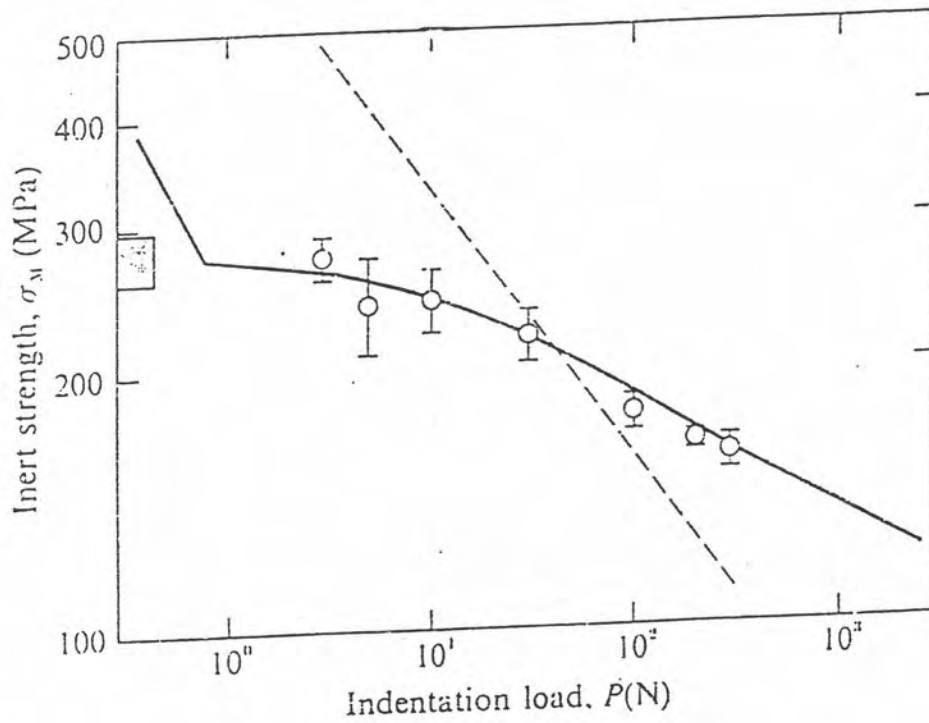
Fig. 3.12 Inert strength results for Vickers indentations in polyctystalline alumina, grain size

35 μm, as function of load. Data points represent confirmed failures from

indentation sites. Error bars designate standard deviation limits.Shaded area at left

indicates data. Dashed line is comparative $\sigma_M \alpha\ P^{-1/3}$ fit to monocrystal sapphire

Relative insensitivity of alumina data to load is measure of `flaw tolerance'.

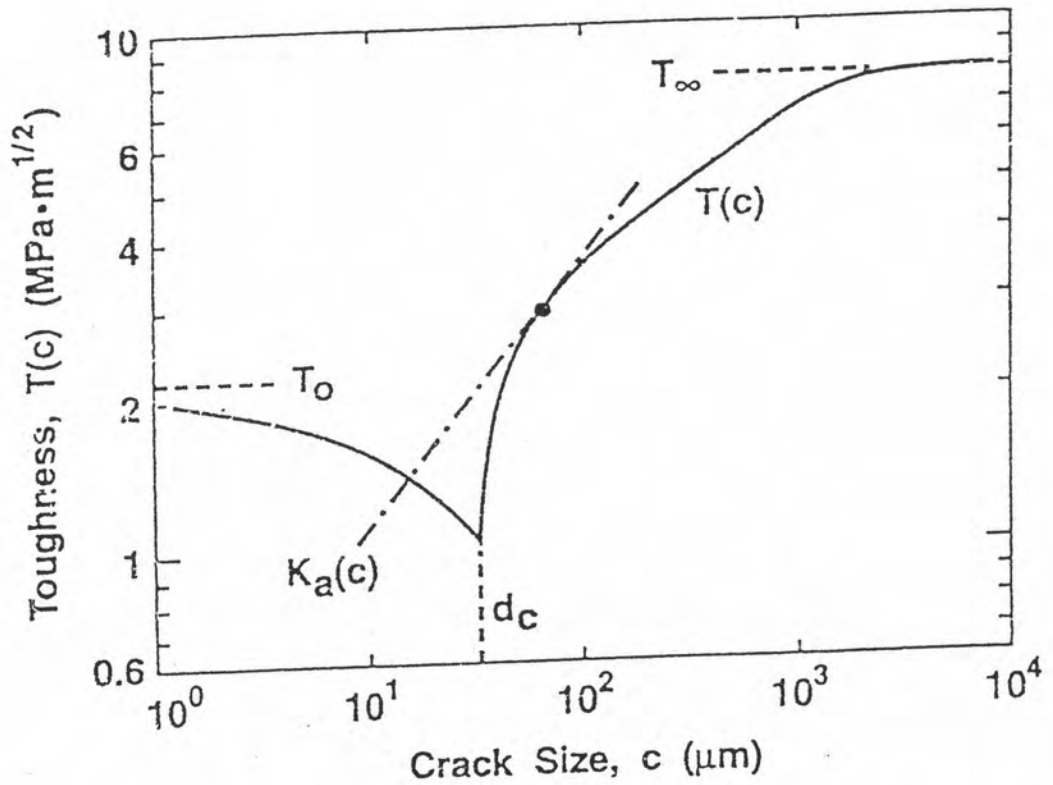(After Mai, Y-W. & Lawn, B.R. (47))

Fig. 3.13 (A) Inert strength as function of Vickers indentation load for a reference single-phase polycrystalline alumina, grain size $l = 23$ μm, tested in dry silicone oil. Shaded region at left represents breaks from natural flaws. Solid curve is fit of bridging T-curve formalism. (b) Deconvoluted T-curve. Dashed line is $K_a(c)$ tangency condition for failure from natural flaw ($\chi = 0$) (After Bennison et al.(50))

dimishing); that at $c > d$ to a dominant $T_\mu(c)$ function (long-crack, negative increasing). Path 1 -> 2 -> 3 -> 4 traces the evalution to failure. The first instability at segment 2 corresponds to pop-in from the indentation crack. That second instability at segment 4 denotes final failure at σ_m. It is the diminished sensitivity to the load-dependent K_r term (which in turn controls the intial crack size at $\sigma_a = 0$ in Fig. 3.14) in the vicinity of this latter barrier that ultimately accounts for the flaw tolerance in Fig. 3.12.

The " calibrated " T-curve contains all the necessary ingredients to predict the effects of variations in microstructural characteristics on the toughness characteristics.

3.5.2 Phase Transformation Stress

The discovery that Zircoria can be subatantially toughned by stress-activated phase transformation as previously described in Sect.1.3 has resulted in fracture mechanics modelling in the early 1980s by Evans and others. We will first investigate the condition for initation of the constrained martensitic transformation, tetragonal -> monoclinic, and then evaluate the ensuing toughness increment.

(i) Initiation of Transformation Again, one may anticipate a threshold particle size for spontaneous transformation. The energy difference between the initial, tetragonal (t), and final, monoclinic (m), states for a particle of radius a is (49)

$$\Delta F = 4/3\pi a^3 \Delta U_E + 4\pi a^2 \Delta U_s \qquad (3.42)$$

with $\Delta U_E = U_E^m - U_E^t$ the differential volume energy density (including chemical energy as well as elastic strain energy of constrained particle) and $\Delta U_s = U_s^m - U_s^t$ the differential surface energy (chemical and configuration components associated with the particle-matrix interface plus energy of any twin interfaces).Then it is thermodynamically permissible for the transformation to proceed when $\Delta F < 0$ which determines the threshold radius
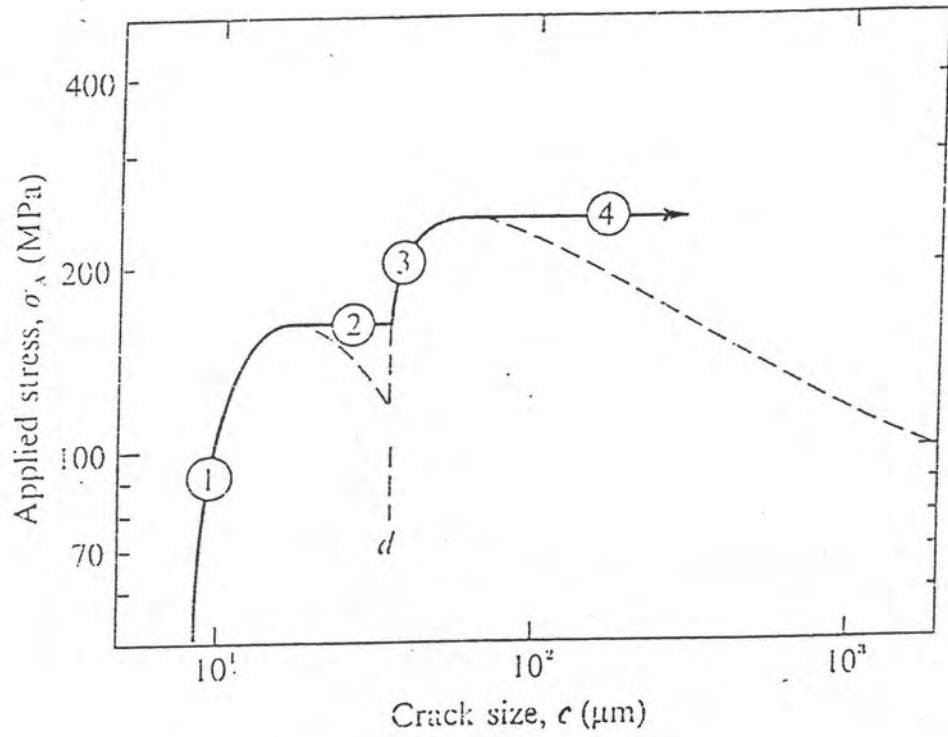
$$a_c = -3\Delta U_E/\Delta U_s \qquad (3.43)$$

Fig. 3.14 Applied stress vs crack size for Vickers indentation in alumina, using parametric

evaluations from Fig.3.12. Calculated for load P = 2 N. Note multiple stable and

unstable branches of the quilibrium curve along path 1 -> 2 -> 3 -> 4 to failure.

(After Mai, Y-W. & Lawn, B.R. (47))

(nothing that, in analogy to cracks, as volume energy is released, $\Delta U_E < 0$, surface energy is gained, $\Delta U_s > 0$).

This argument is at best incomplete, for it makes no statement as to the reaction path between the end points, specifically to the existence of intervening energy barriers. The condition $\Delta F < 0$ is therefore a necessary but not sufficient condition for the transformation, so Eq.(3.43) is a lower bound. Nevertheless, the notion of a threshold particle radius prevails. Indeed, size effects are characteristic of any process where the energetics balance volume and surface terms. The field of a primary crack can activate transformation at $a < a_c$. However, McMeeking and Evans have proven that the initial transformation does not change the crack-tip stress intensity factor and thus has no influence on the fracture toughness (6)

(ii) Toughness Increment

Consider a dilation frontal zone around the crack tip, with persistent influence in a wake layer, body stresses σ_μ and strains ε_μ within such a zone are defined by a constitutive relation $\sigma_\mu(\varepsilon_\mu)$, Fig.3.15a. The stress-strain curve is hysteretic, corresponding to a residual dilation in the wake. An indication of $\sigma_\mu(x)$ and $\varepsilon_\mu(x)$ for volume elements on a plane $y = $ const. intersecting the frontal zone is given in Fig. 3.15(b). The zone width w defines a boundary outside of which volume elements remain on the elastic portion of the $\sigma_\mu(\varepsilon_\mu)$ curve.

Again, the configuration can be treated in terms of J-integral. So the internal material resistance becomes (49)

$$R = 2w \int_0^{\varepsilon_\mu} \sigma_\mu(\varepsilon_\mu)d\varepsilon_\mu \qquad (3.44)$$

The energetics of shielding are governed by the area under a constitute, $\sigma_\mu(\varepsilon_\mu)$ curve. In principle, given this curve, to obtaining a solution for σ_μ, only the size W of dilation zone is needed. In reality, matters are somewhat more complicated. By allowing the system to unload
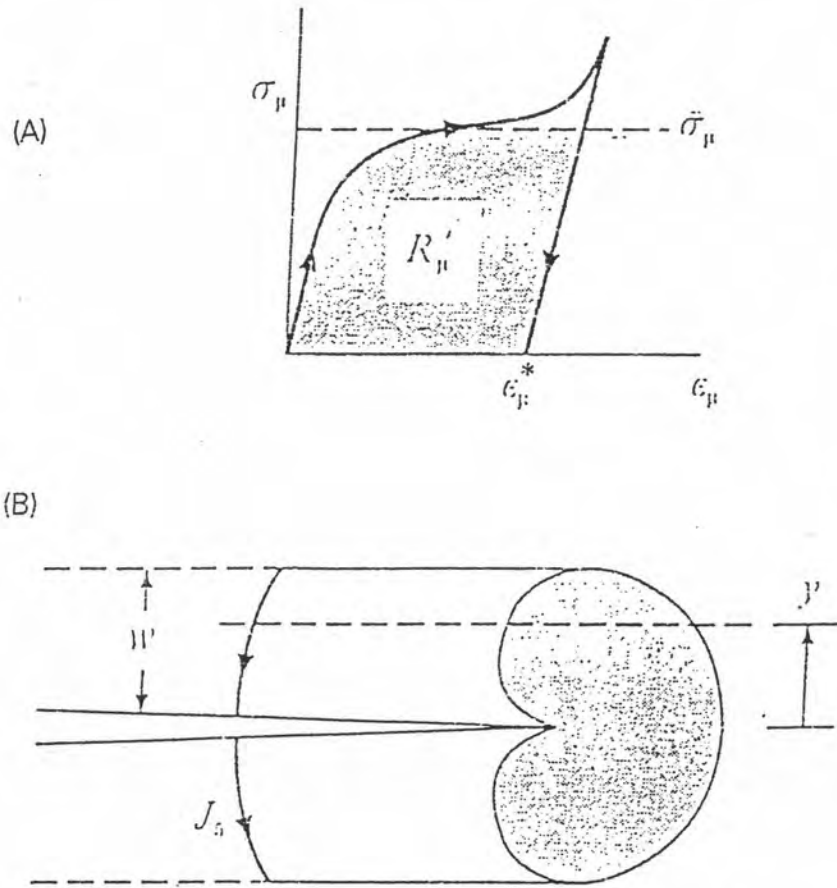
Fig. 3.15 Shielding by frontal-zone dilation. (A) Stress-strain function σ_μ $(\varepsilon_\mu : \sigma_\mu$ is 'averaged' stress and ε^*_μ residual strain. (B) J-integral contours through wake. Distributuins of dilation stresses $\sigma_\mu(\chi)$ and strains $\varepsilon_\mu(\chi)$ along plane y = const indicated at bottom. Area under curve in (a) determines steady-state increment in crack-resistance energy.

hysteretically in stress-strain space (Fig.3.15a),it seems to be exceeded the conditions for validily of the J-integral.

There are also subtle questions concerning how the zone develops. Steady state is straight forward. The wake is well-established (Fig.3.16c), and the critical stress σ_c^T and appropriate upper limit $\varepsilon_\mu = \varepsilon^T$ in the integral are independertly determinable from the constitutive micromechanics of the dilation process. The corresponding limiting zone size $w = w_c$ may be estimated (if only approximately) from solutions of the elastic near field. Thus the steady-state resistance $R_\infty = R_0 = R\mu^\infty = $ const. (and corresponding T_∞, $R_0 = $ intrinsic material resistance) can be determined from

$$R\mu^\infty = 2\sigma_c^T \varepsilon^T w_c \quad \text{(steady state).} \tag{3.45}$$

where σ_c^T is the critical dilation stress and $\varepsilon^T \approx e^T V_f$ is the net wake transformation strain, with $e^T = $ the unconstrained dilation strain of a single tranformation particle and V_f the volume fraction of particles. Similarly, the weak-shielding zone width is

$$w_c = \Omega_T (T_\infty / \sigma_c^T)^2 \tag{3.46}$$

with $\Omega_T = (1/2\pi) f_{ii}^2 (\theta_T) \sin\theta_T (\theta_T = 60^\circ$ at furthere most tangency point) = 0.062.
So the steady-state resistance is

$$R_\infty = R_0 (1 + 2\Omega_T e^T V_f E' / \sigma_c^T), \text{ (weak shielding)} \tag{3.47}$$

approximately, with E' the composite modulus.

For the transient state, matter are much more complex. The evolution is depicted schematically in Fig.3.16. An expanding dilation zone along the front of an initially stationary crack, state a, makes no contribution to the shielding. That arises because the dilated element ahead of the crack ($\theta < 60^\circ$) exert tensile (hoop) opening stresses on the crack plane, while
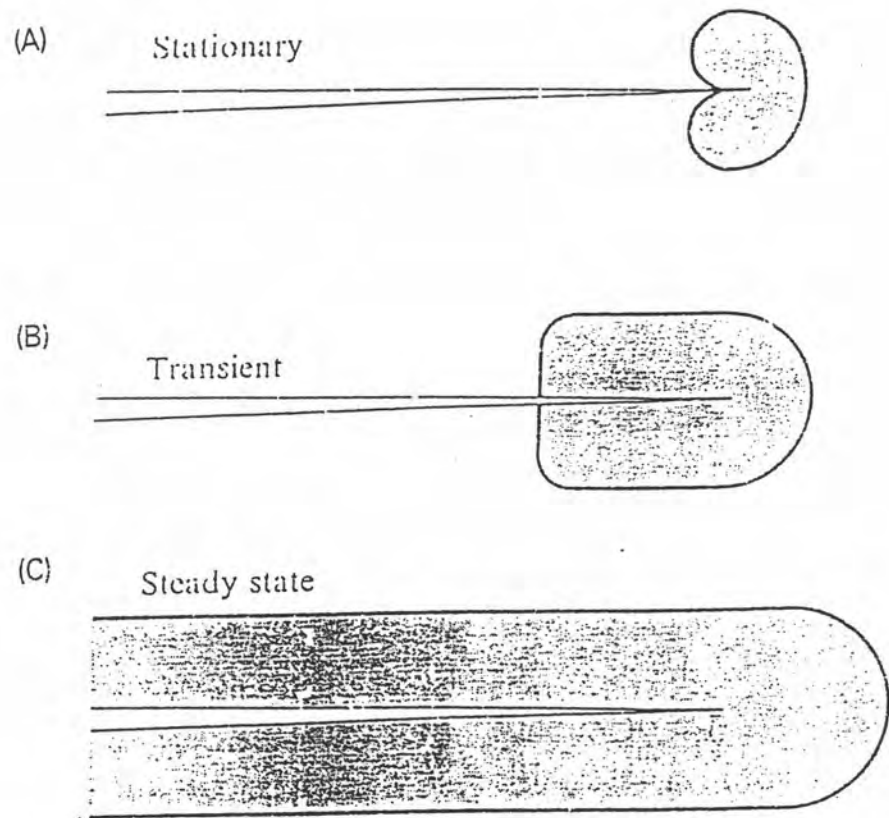
Fig. 3.16 Development of frontal-wake zone with crack extension : (A) zero extension, equilibrium frontal zone, $R = R_0$ ($T = T_0$); (B) short extension, partial wake, $R = R_0 + R_\mu$ ($T = T_0 + T_\mu$); (C) long extension, steady-state wake, $R_\infty = R_0 + R^\infty_\mu$ ($T_\infty = T_0 + T^\infty_\mu$).

adjacent and behind $(\theta > 60^\circ)$ exert compressive (radial) closure stresses; the net effect at equilubrium is cancellation. At a critical zone size the crack begins to propagate, state b, creating an imbalance in closure stresses from the irreversibly unloaded particles in the expanding wake, so the toughness begin to increase. Ultimately, after the crack has extended sufficiently that the wake is fully-developed, state c , the intensity of closure stresses saturates, and steady steady state obtains. The transient problem has been treated by McMeeking and Evans (6),in the approximation of an ever-constant wake width $w = w_c$, by integrating over the transformation zone boundary in a stress-intensity analysis of the toughness increment,

$$T_\mu(\Delta c) = \eta\, E\varepsilon^T w_c^{1/2} \phi(\Delta c/w_c) \qquad\qquad (3.48)$$

when $\eta = 1/3^{1/4} 2\pi^{1/2}(1-\gamma) \approx 0.28$ and $\phi(\Delta c/w_c)$ is a (numerically evaluated) dimensionless function of crack extension. This last function is monotonic with limits $\phi = 0$ at $\Delta c = 0$ (no wake) and $\phi = 1$ at $\Delta c \gg w_c$ (steady state),as reflected directly in the data of Fig, 3.17 .
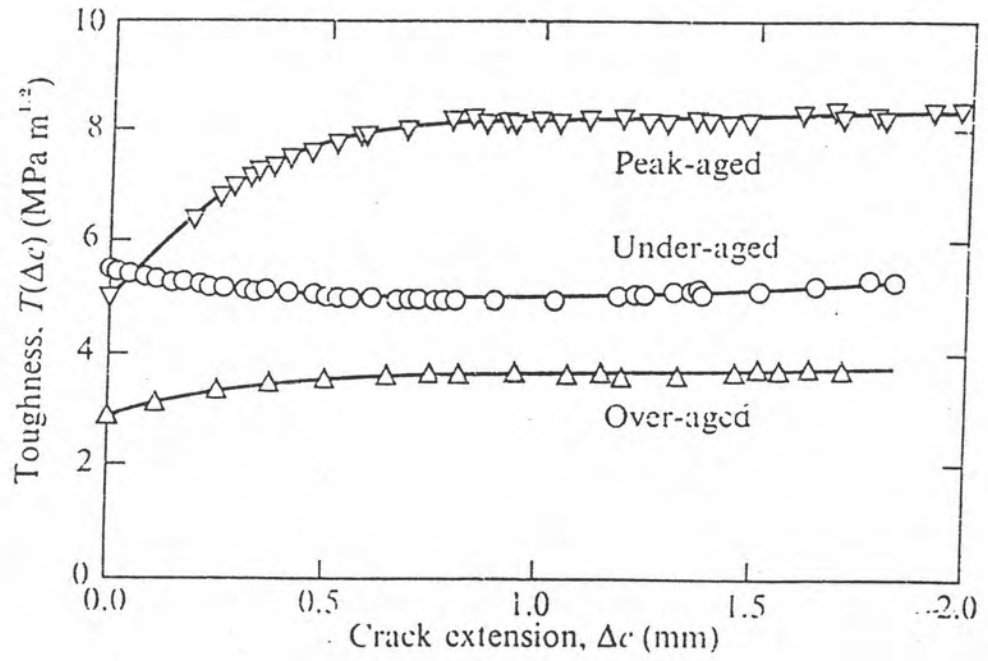
Fig. 3.17 Measured toughness curves for Mg-PSZ, under-aged, peak-aged, over-aged.
CT specimens. (After A.H. Heuer et al (51))